Pre-Test CFD for the Design and Execution of the Enhanced Injection and Mixing Project at NASA Langley Research Center

Tomasz G. Drozda, Erik L. Axdahl, and Karen F. Cabell
NASA Langley Research Center
Hampton, Virginia

ABSTRACT

With the increasing costs of physics experiments and simultaneous increase in availability and maturity of computational tools it is not surprising that computational fluid dynamics (CFD) is playing an increasingly important role, not only in post-test investigations, but also in the early stages of experimental planning. This paper describes a CFD-based effort executed in close collaboration between computational fluid dynamicists and experimentalists to develop a virtual experiment during the early planning stages of the Enhanced Injection and Mixing project at NASA Langley Research Center. This projects aims to investigate supersonic combustion ramjet (scramjet) fuel injection and mixing physics, improve the understanding of underlying physical processes, and develop enhancement strategies and functional relationships relevant to flight Mach numbers greater than 8. The purpose of the virtual experiment was to provide flow field data to aid in the design of the experimental apparatus and the in-stream rake probes, to verify the non-intrusive measurements based on NO-PLIF, and to perform pre-test analysis of quantities obtainable from the experiment and CFD. The approach also allowed for the joint team to develop common data processing and analysis tools, and to test research ideas. The virtual experiment consisted of a series of Reynolds-averaged simulations (RAS). These simulations included the facility nozzle, the experimental apparatus with a baseline strut injector, and the test cabin. Pure helium and helium-air mixtures were used to determine the efficacy of different inert gases to model hydrogen injection. The results of the simulations were analyzed by computing mixing efficiency, total pressure recovery, and stream thrust potential. As the experimental effort progresses, the simulation results will be compared with the experimental data to calibrate the modeling constants present in the CFD and validate simulation fidelity. CFD will also be used to investigate different injector concepts, improve understanding of the flow structure and flow physics, and develop functional relationships. Both RAS and large eddy simulations (LES) are planned for post-test analysis of the experimental data.

INTRODUCTION

The increasing costs of facility operations and safety requirements often lead to an increase in the overall financial and schedule costs of new physics experiments. The simultaneous increase in the ubiquity, availability, and maturity of computational tools allows for their relatively rapid and inexpensive deployment because the costs of computational facilities are typically distributed broadly across organizations. Furthermore, the maturity of physics models present in current computational tools, and repeated successes with their use over time, have raised confidence in the resulting data to levels where a subject matter expert utilizing numerical simulations can now deploy these tools to answer many lingering questions before any experimental apparatus is built. Despite this, both designers and simulation experts generally agree that to support the design processes for practical devices, experimentation is still required to provide both real-life data and validate computational models. In combination, the above factors result in computational tools playing an increasingly important role in the early stages of experimental planning and post-test investigations with experimental data still required to fully vet the results of the latter.

The current work describes a case where computational fluid dynamics (CFD) tools have been heavily leveraged in the design and development of the Enhanced Injection and Mixing (EIM) project.[1] This project aims at studying fundamental physics of fuel injection and mixing processes in a supersonic combustion ramjet (scramjet) in the absence of heat release at flight Mach numbers greater than 8. The CFD here consists of Reynolds-averaged simulations (RAS) which utilize conventional and well-understood turbulence models and are applied following experience-based best practices for the problems of interest. This is a key aspect because no experimental data is yet available for these conditions.

The paper is organized as follows. First, a general description is offered of the EIM project as relevant to this work. Next, a description of numerical considerations is provided that apply to all simulations presented herein. Any deviations from these considerations are described within the subsequent sections pertaining to numerical simulations of the specific configuration. These configurations consist of the facility nozzle, a baseline strut injector, and experimental apparatus in the test cabin. The impact of each numerical configuration on the experimental design process are described within each of the respective sections. The paper is then summarized and several ongoing and future efforts are described.

ENHANCED INJECTION AND MIXING PROJECT

The Enhanced Injection and Mixing (EIM) project, conducted in the NASA Langley Arc-Heated Scramjet Test Facility (AHSTF), entails testing of various fuel injection devices mounted on an open flat plate located downstream of a Mach 6 facility nozzle which simulates the combustor entrance of a flight vehicle traveling at a Mach number of about 14 to 16. Current experiments focus on studying fuel injection and mixing processes in the absence of heat release by utilizing helium as a fuel simulant. Figure 1 shows the cross section of the experimental apparatus mounted in the test cabin. Noted on the figure are the flat plate test bed platform with its leading edge positioned several inches below the top wall of the Mach 6 facility nozzle. Also noted are the in-stream rake traverse system, jet stretchers, and the instrumentation shroud located on the back side of the flat plate. The dash lines denote the outline of the facility viewing windows located on each side of the test cabin. The figure shows the orientation of the experimental apparatus as is installed in the wind tunnel facility, however, it should be noted that in all subsequent CFD simulations the positive y-direction is oriented in the plate-normal direction, which is pointing toward the ground.

Two total temperature conditions are investigated: the lower value is set high enough to prevent condensation of the oxygen in the facility air after expansion through the facility nozzle and is equal to 1310 R; the higher value is limited by a requirement for uncooled hardware and is equal to 1760 R. The total pressure for both cases is set to 625 psia which corresponds to the maximum value supported by the facility.

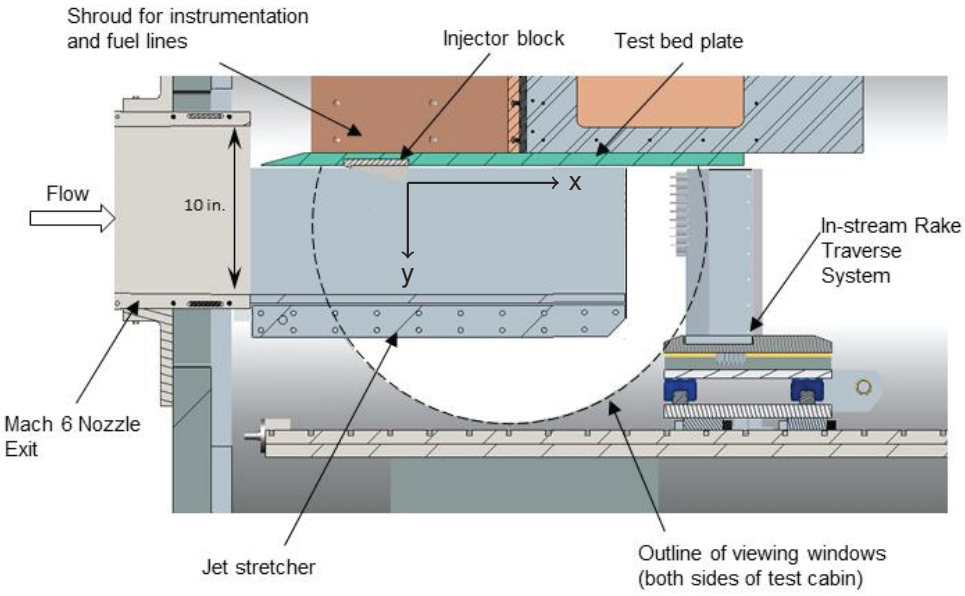

Figure 1: Cross section of the experimental cabin with the facility nozzle, test bed plate, jet-stretchers, instrumentation shroud, and the in-stream rake probe indicated. The figure shows the configuration as installed in the wind tunnel, however, all CFD simulations were performed with the positive y-direction in the plate-normal direction, which is pointing toward the ground.

The experiment is intended to provide a test-bed flexible enough for testing a variety of different fuel injector devices and injection strategies. The experimental measurements consist of wall-based pressure and temperature data and in-stream fuel mole fraction, Pitot pressure, and total temperature data. Flow visualization is provided by the NO-PLIF technique.[2,3] CFD data are obtained using RAS which are further post-processed to compute injection performance metrics for each injection strategy. Currently, the mixing efficiency, total pressure recovery, and stream thrust potential are used. The most promising injector configurations will be simulated via large-eddy simulations (LES), which although computationally more expensive than RAS, provide, in addition to steady-state properties obtained by time-averaging, the unsteady flow details. It is expected that the LES will provide improved accuracy over RAS, especially for configurations with multiple geometry-induced large flow scales, flow separations, and recirculations zones. At the very least, the LES will provide a means of validating the performance of RAS for such flows. The LES will also be considered for cases where the unsteady effects are explicitly included, such as with pulsed injection, for example.

Specific objectives of the EIM project are enumerated below.

1. To increase knowledge and understanding of the fundamental physics governing fuel-air mixing relevant to the hypervelocity flight regime.
2. To develop strategies for improving injector performance (increased mixing efficiency, reduced losses and drag).
3. To develop the functional relationships between mixing efficiency, losses (i.e total pressure loss and drag) and flowpath geometry.

The payoff and impact of meeting these objectives is higher performance scramjet propulsion systems operating at higher Mach number flight conditions. Further details of the project are provided by Cabell et al.[1]

NUMERICAL CONSIDERATIONS

The numerical simulations were performed using the Viscous Upwind aLgorithm for Complex flow ANalysis (VULCAN-CFD) code.[4] VULCAN-CFD is a multi-block; structured-grid, cell-centered, finite-volume solver widely used for all-speed flow simulations. For this work, Reynolds-averaged simulations (RAS) were performed. The advective terms were computed using a MUSCL scheme[5] with the Low-Dissipation Flux-Split Scheme (LDFSS) of Edwards.[6] A non-reacting, thermally perfect mixture of 21% oxygen (O_2), 78% nitrogen (N_2), and 1% nitric oxide (NO) was used for the facility air. A small amount of NO was present to account for production of this species in the arc-heater of the experimental facility.[7] The thermodynamic properties of mixture components were computed using curve fits of McBride et al.[8] For calculations utilizing the thermodynamic non-equilibrium model, these curve fits are evaluated at the vibrational temperature .[9] The governing equations were integrated using an implicit diagonalized approximate factorization (DAF) method.[10] The current work used the baseline blended $k-\omega/k-\epsilon$ turbulent physics model of Menter.[11] The Reynolds heat and species mass fluxes were modeled using a gradient diffusion model with turbulent Prandtl and Schmidt numbers of 0.9 and 0.5, respectively. Wilcox wall matching functions[12] were also used, where appropriate, to reduce the near-wall grid resolution requirements. A grid sensitivity study was performed for each simulation with negligible changes in flow properties being computed when the grid resolution was changed (usually reduced) by a factor of two in each direction. All simulations were converged until the total integrated mass flow rate and the total integrated heat flux on the walls remained constant. This typically occurred when the value of the L_2-norm of the steady-state equation-set residual decreased by about 3-4 orders of magnitude.

FACILITY NOZZLE SIMULATIONS

The Mach 6 facility nozzle used in the current experiment was designed to minimize the core flow non-uniformities for Mach 7 flight enthalpy, free-jet experiments in the AHSTF.[13] However, the conditions of interest to the EIM project are off-design, and no experimental data about the nozzle's flow quality are available. In order to determine the extent of the core flow and its properties, three dimensional (3D) RAS of the facility nozzle were conducted. The simulations of the facility nozzle were used to:

- determine the extent of the core flow and therefore the maximum size of the injection device to be tested downstream;
- determine properties at the nozzle's exit plane for the cases corresponding to the two values of the total enthalpy considered by the EIM;
- determine the vertical position of the experimental flat plate within the core flow;
- provide data to verify NO-PLIF measurements;
- and assess the impact of thermodynamic non-equilibrium on the flow field properties.

The following discussion describes the facility nozzle and the simulations performed to address the above listed items.

The facility nozzle used in the current experiments has a rectangular cross-section with a square exit of 10x10 inches. Taking advantage of the nozzle symmetries, only a quarter of the full nozzle geometry was simulated. The quarter-geometry grid consisted of about 3.9 million cells. Subsonic inflow boundary conditions specifying a total pressure of 625 psia and temperature of 1730 R were used at the inflow located upstream of the nozzle throat for the high enthalpy case. For the low enthalpy case, a total pressure of 625 psia and temperature of 1310 R were used. First-order extrapolation was used at the supersonic outflow of the nozzle. The walls were modeled using a no-slip boundary condition for the velocities. The y+ values ranged from about 10 to 80, with the average of about 25 and the largest values located upstream and at the nozzle throat. The temperatures at the nozzle walls were obtained by locally solving a one-dimensional, steady-state, heat conduction equation with the experimentally-obtained average values of the

Table 1: Flow conditions at the center line of the facility nozzle exit plane obtained from 3D RAS simulations.

Property	Low Enthalpy	High Enthalpy
Mach	6.41	6.36
Total Pressure (psia)	625.75	625.75
Total Temperature (R)	1310.6	1732.2
Pressure (psia)	0.2572	0.2630
Temperature (R)	145.2	198.9

nozzle outer-wall temperatures as an input. The flow was initialized using a solution of the one-dimensional isentropic and adiabatic converging-diverging nozzle problem.

Figure 2 shows the contours of the Mach number, total pressure, and total temperature with the left and right columns, corresponding to the low and high values of the total enthalpy, respectively. Visual inspection reveals the two flow fields are quite similar. The flow passing through the facility nozzle, not only expands, but also develops relatively thick (about 1.5 in.) boundary layers. A slight thickening of about 0.125-0.25 in. of the boundary layer may be noted in the simulations corresponding to the higher value of the total enthalpy. These boundary layers reduce the size of the exit core flow. At the exit plane of each figure, a half-square box denotes the core flow chosen for this experiment. The box size is 5x5 inches and is determined by examining the exit profiles of the facility nozzle, shown in Fig. 3. This figure shows the profiles of the Mach number, total pressure, and total temperature along the y- and z-direction center lines of the nozzle. The y-direction profiles of the total temperature remain about constant over the most narrow span of the core flow. Therefore, by visual inspection, the core flow is determined to approximately span a distance ranging from -2.5 in. to 2.5 in. along the y-direction. Although, upon close examination, these steady-state profiles appear to offer an additional 0.5-1 in. or so more of core flow in either direction, the stated range is chosen to be conservative. For the purpose of designing the experiment the z-direction range is set to match the y-direction resulting in a square cross-sectional area over which experiments could be conducted. The vertical placement of the experimental flat plate is chosen to maximize the extent of core flow over the apparatus. Therefore, based on the determined conservative extent of the core flow, the leading edge of the flat plate is placed -2.5 in. in the y-direction from the center line of the facility nozzle. The placement of the flat plate together with the selected size of the core flow set limits on the size and number of the injectors that can be tested downstream.

The facility nozzle center line conditions for both the low and high total enthalpy cases are shown in Table 1. It should be noted that RAS predicted a larger value (by 0.1%) of the total pressure at the center line of the exit plane of the facility nozzle than is found in the plenum. A value larger than the plenum total pressure would in general indicate unphysical behavior if adiabatic nozzle walls were used in the simulations. However, in the current simulations, this total pressure rise occurs through, and just downstream of, the facility nozzle throat where a water-cooled wall section is being modeled by the CFD. The effects of water-cooling on the facility nozzle wall may be observed by examining the dark area near the nozzle throat in the contour plots of the total temperature in Fig. 2. While cooling does increase the total pressure, such a low level of total pressure rise may also be attributed to the numerical accuracy of the computational scheme. Discerning the contribution of either of these two factors would require additional simulations. Because the rise in the value of the total pressure was small, additional calculations were not performed and the value of the total pressure was accepted as within reasonable accuracy for the pre-test simulations.

The results of the facility nozzle simulations were also compared with data obtained from the NO-PLIF flow visualization technique as previously reported by Kidd III et al.[3] In their analysis, they utilized RAS static temperature data obtained at the exit plane of the facility nozzle to verify the values of the temperature obtained using the NO-PLIF technique. In general, the difference between experimental and CFD data was found to be within 1-7%, with the CFD overpredicting the experimental values. However, it should be noted that the CFD calculations were not rerun to match exactly the values of the total pressure and total temperature observed experimentally during the NO-PLIF checkout tests. Furthermore, the 3D RAS of the facility nozzle utilized a thermodynamic equilibrium model. When thermodynamic non-equilibrium

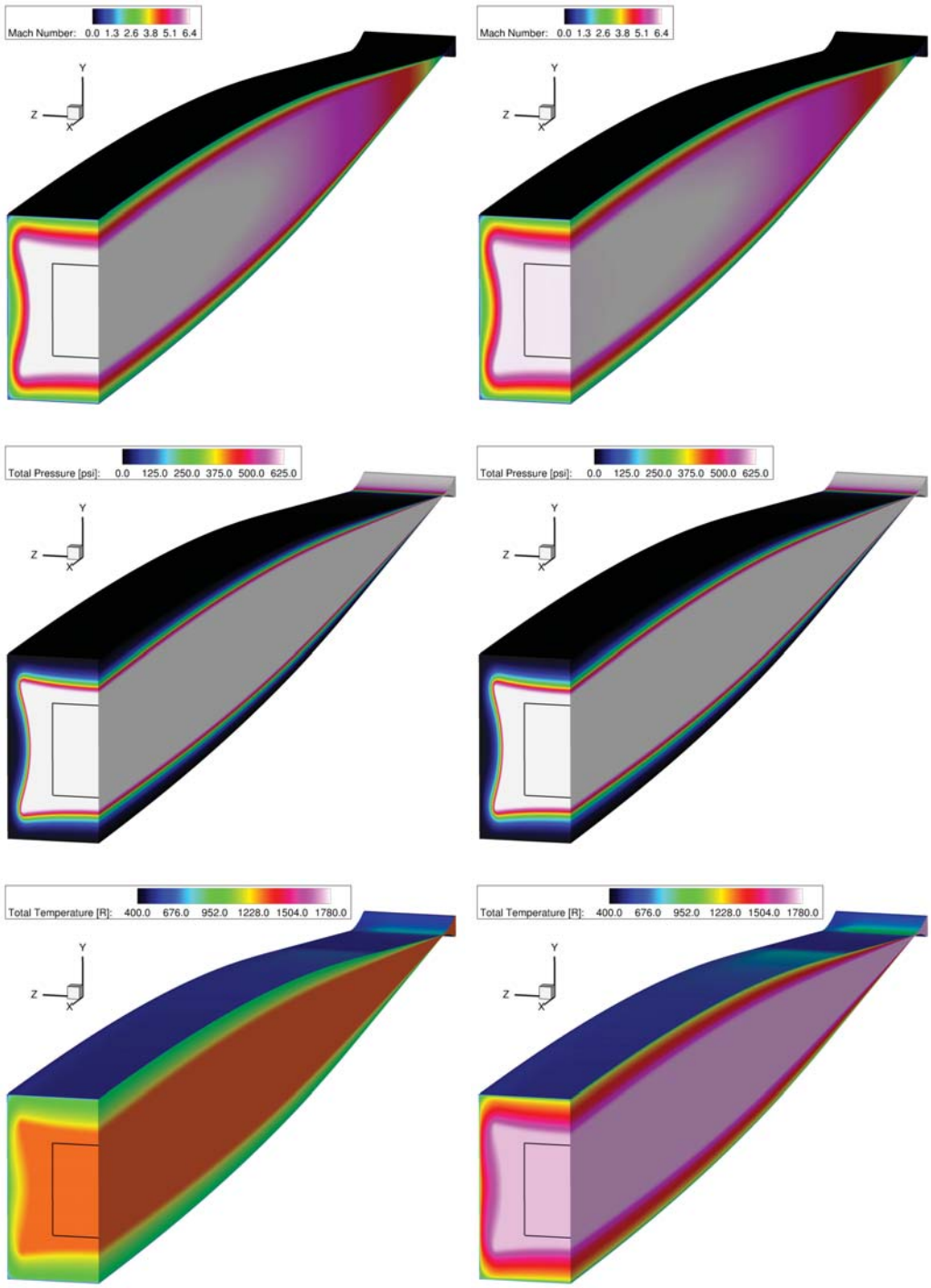

Figure 2: Contours of the Mach number, total pressure, and total temperature, obtained using 3D RAS of the facility nozzle at the low (left column) and high (right column) values of the total enthalpy.

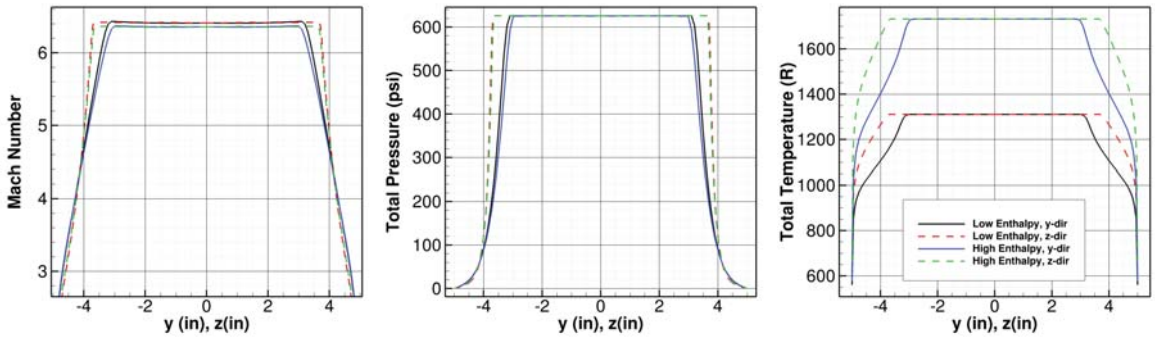

Figure 3: Profiles of the Mach number, total pressure, and total temperature along the y- and z-direction center lines at the facility nozzle exit plane for the low- and high-values of the total enthalpy obtained using 3D RAS.

effects were included, as discussed next, the CFD produced a reduction of up to 5% in the value of the static temperature. Nevertheless, these relatively successful comparisons between NO-PLIF data and the pre-test CFD provided confidence in the setup and data analysis of the NO-PLIF system.

The above discrepancies between the CFD predictions and the NO-PLIF measurements of the static temperature, as well as, other discrepancies between CFD and experimental measurements[9,14] observed for other facility nozzles operating at a higher value of the total enthalpy, suggest the possibility of a flow in thermodynamic vibrational non-equilibrium. Although these effects are expected to decrease with decreasing total enthalpy, CFD can be used to explicitly assess this at the total temperature conditions of interest to the EIM project. For this purpose a two dimensional (2D) RAS of the facility nozzle has been performed. In order to determine the upper bound of the impact of the vibrational non-equilibrium effects, only the high value of the total temperature was considered together with adiabatic wall boundary conditions. Subsonic inflow boundary conditions, specifying a total pressure of 625 psia and temperature of 1730 R were used at the facility nozzle inflow located upstream of the nozzle throat. Because the nozzle inflow plane in the current simulations is located downstream of the facility nozzle plenum, the inflow conditions were assumed to be in thermodynamic equilibrium. Therefore, any thermodynamic non-equilibrium effects are a result of rapidly accelerating the flow through the converging-diverging nozzle. First-order extrapolation was used at the supersonic outflow of the nozzle. The details of the thermodynamic vibrational non-equilibrium model used in the current simulations are described by Baurle.[9]

Figure 4 shows the contours of the Mach number obtained using 2D RAS for the thermodynamic equilibrium and non-equilibrium cases. The expansion processes are nearly indistinguishable to the eye albeit some shift in values of the Mach number to the left can be observed. This indicates that, for a given nozzle cross-sectional area, the flow expands to a higher value of the Mach number when thermodynamic non-equilibrium is taken into account. Figure 5 shows the profiles of the Mach number, static pressure, and static translational-rotational temperature at the exit plane of the facility nozzle highlighting the differences between the values obtained using the thermodynamic equilibrium and non-equilibrium models. Consistent with the visual observations of Fig. 4, the value of the Mach number when thermodynamic non-equilibrium is considered increases by about 1% with respect to the equilibrium value. Consequently, the values of the static pressure and temperature decrease by about 3% and 5%, respectively. The thermodynamic non-equilibrium model was not implemented in the VULCAN-CFD code in the early development stages of the experiment. As a result, thermodynamic non-equilibrium simulations were performed much later in the project with all the other simulations described herein using thermodynamic equilibrium. Nevertheless, the relatively small differences between results obtained using the thermodynamic equilibrium and non-equilibrium models validate the use of the equilibrium model for the pre-test design work. However, post-test simulations performed at specific, experimentally-obtained, total pressure and temperature conditions

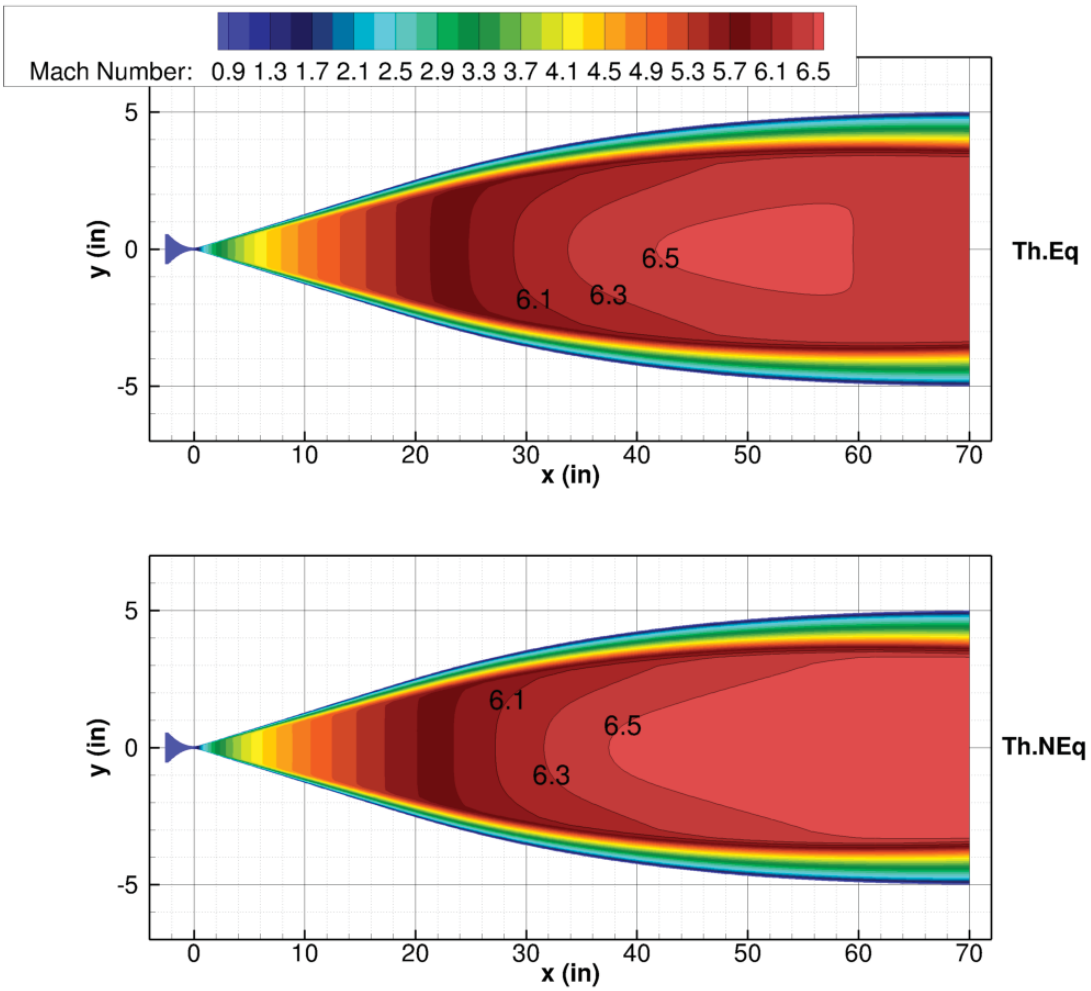

Figure 4: Contours of the Mach number obtained using thermodynamic equilibrium (Th.Eq) and non-equilibrium (Th.NEq) models, respectively, using 2D RAS of the facility nozzle.

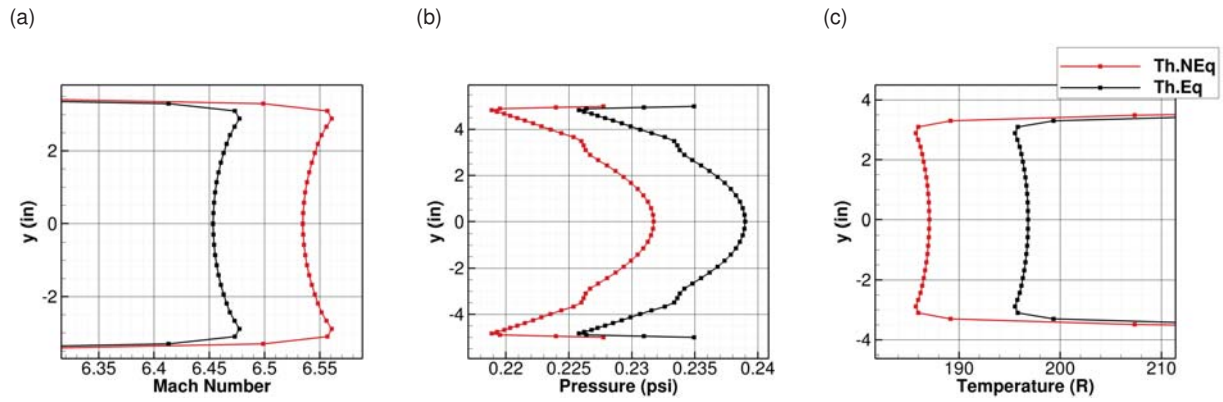

Figure 5: Profiles of the Mach number, static pressure and static translational-rotational temperature at the exit of the facility nozzle and obtained using thermodynamic equilibrium (Th.Eq) and non-equilibrium (Th.NEq) models, respectively, using 2D RAS.

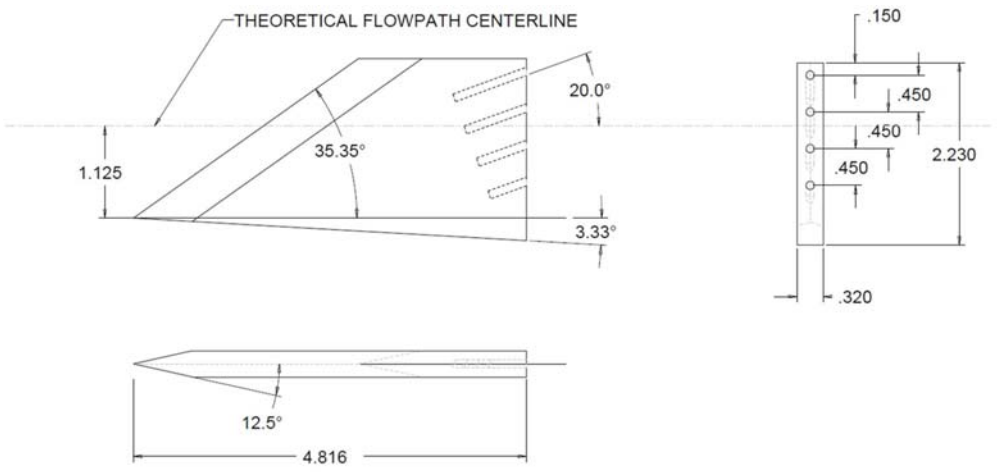

Figure 6: Schematic of the baseline strut injector used in the pre-test simulations.

will utilize the thermodynamic non-equilibrium model to more closely represent relevant physics of the flow field.

BASELINE STRUT INJECTOR SIMULATIONS

The 3D RAS of the facility nozzle provided key information about the properties of the facility nozzle core flow, as well as, established the position of the flat plate within this core flow. The next set of simulations involved a typical strut injector and were used to:

- provide comparative operational information about the use of different fuel simulants;
- provide information about the temperature and heat fluxes at the surface of the flat plate for thermal analysis of the apparatus;
- provide the aerodynamic properties and the mixing flow field for the design of the in-stream gas sampling rake probe;
- develop and verify post-processing and analysis tools before experimental data was available.

The following discussion describes the details of the strut injector and related simulations performed to address the above listed items.

A strut injector previously studied by Baurle et al.[15] at Mach 4.5, cold flow, combustor conditions was selected as a baseline. This choice was motivated by the fact that in high Mach number flight it is increasingly difficult to penetrate the core flow of the flowpath and a fuel placement device, such as a strut, may be required. Furthermore, the axial momentum provided by the fuel is expected to offset some of the drag losses generated by the injector body. The size of this injector also fit well within the 5x5 test area determined from the facility nozzle simulations. The strut was modified from the configuration studied by Baurle et al.[15] by adding a fourth fuel port, removing of adjacent interdigitated injectors, and re-aligning of all the injector ports in the same direction. Specifically, removal of the interdigitated injectors effectively doubled the distance between adjacent injectors. A schematic of the modified injector is shown in Fig. 6.

An array of injectors was envisioned for the experiment. In order to reduce the computational cost, the flow was assumed to be symmetric about the center plane of the injector and about the mid plane between adjacent injectors. The computational grid consisted of about 30 million cells. The current simulations used an integrate-to-the-wall grid. While more computationally expensive, such grids are expected to pro-

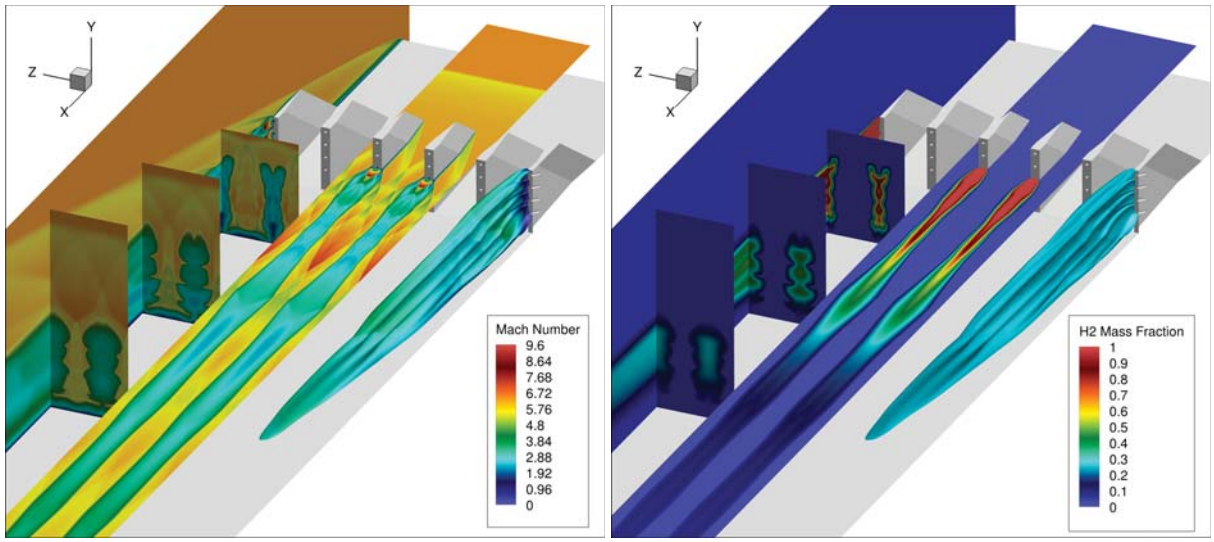

Figure 7: Contours of Mach number and hydrogen mass fraction along the injector center line and several cross-stream and stream-wise planes. Also shown are the iso-surfaces of hydrogen mass fraction colored by the respective quantity in each plot.

vide improved predictions for the heat fluxes at the flat plate surface which were needed for the thermal analysis. Two simulations were performed to support the thermal analysis. Each utilized either adiabatic or isothermal non-slip wall boundary conditions for the flat plate with the isothermal temperature set to 1000 R, as requested by the thermal analyst. The injector body was modeled with adiabatic non-slip walls. The uniform supersonic inflow boundary conditions were obtained from the 3D RAS of the facility nozzle simulations as summarized in Table 1. First-order extrapolation was used at the supersonic outflow. Hydrogen, helium, and a 25%-75% helium-air mixture were used as the fuel and fuel-simulants, respectively, with the mass flow rate set to match that of hydrogen at a specified equivalence ratio (ER) and the flow rate of air computed based on the strut injector's intended fueling cross-sectional area. Helium was considered as a fuel-simulant because its molecular weight most closely matches that of hydrogen gas which is the expected fuel for the flight regime of interest. Helium-air mixtures were considered because the mixture ratio of specific heats better matches that of hydrogen gas.

Figure 7 shows an example calculation corresponding to the high value of the total enthalpy and equivalence ratio of one. While this example plot uses hydrogen as a fuel with chemical reactions computationally disabled, in the actual experiments helium or helium-air would be used as a fuel-simulant. Several contour planes are shown on this figure. These contours qualitatively illustrate the extent of mixing and injector-to-injector interactions downstream of the baseline strut injector. As can be seen, the injector-to-injector mixing plume interactions are quite limited because of large separation between adjacent injectors. This allows for studying of the impact of the shocks, expansions, and vortical flow structures generated by the individual and adjacent injectors' bodies on the individual mixing plumes in the absence of any plume merging.

Figures 8 and 9 show contours of Mach number and mass fraction, respectively, along the center plane of the baseline injector for hydrogen, helium, and helium-air mixture with ER of 1. The case with helium at an ER of 0.1 is also shown and will be discussed below. The Mach number contours in Fig. 8 reveal a complex patter of shocks. These shocks originate at the leading edges of the strut injectors and refract through the fuel plumes of adjacent injectors. Figure 9 shows the contours of the mass fractions of different fuel-simulants. All of the plumes exhibit finger-like mixing patterns that originate at the individual fuel ports and diffuse into the surrounding high-speed air. The stoichiometric mass fraction of hydrogen in the simulated facility air containing 1% NO is equal to 0.0285, therefore the fuel is still quite unmixed even near the end of the plate. It should be noted, however, that the baseline injector is not intended to be an optimal mixer.

(a) 100% H2, ER=1.0

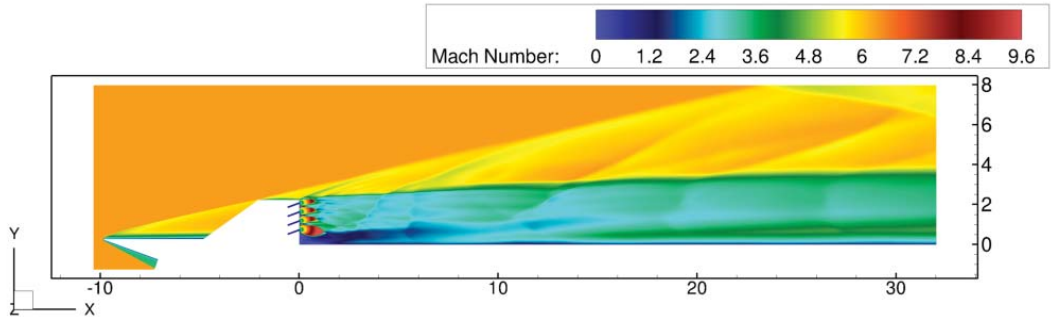

(b) 100% He, ER=1.0

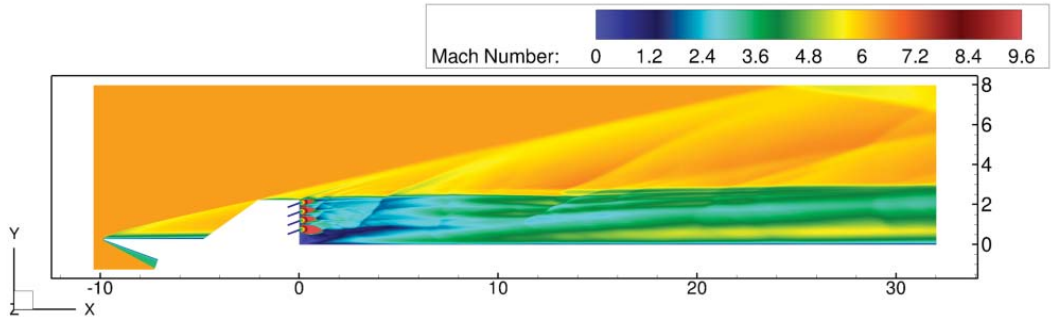

(c) 25%-75% He-Air, ER=1.0

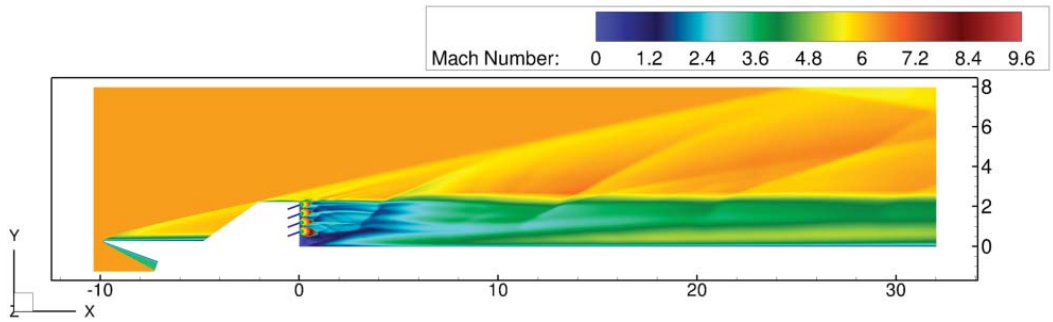

(d) 100% He, ER=0.1

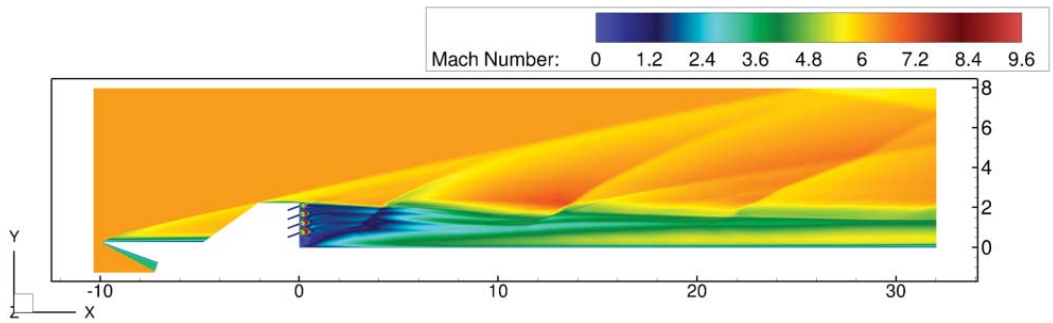

Figure 8: Contours of Mach number for several different fuel-simulants and different values of ER. Plot axis are in inches.

(a) 100% H2, ER=1.0

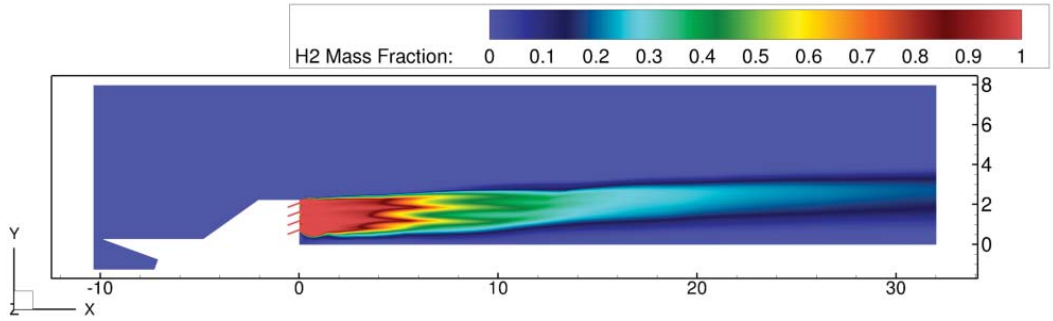

(b) 100% He, ER=1.0

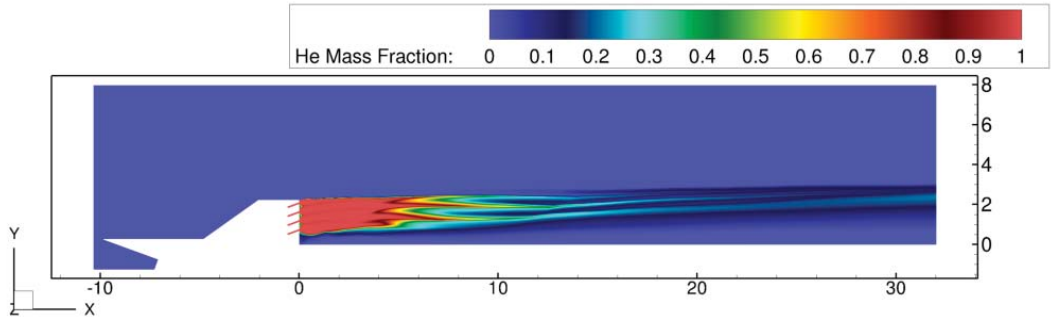

(c) 25%-75% He-Air, ER=1.0

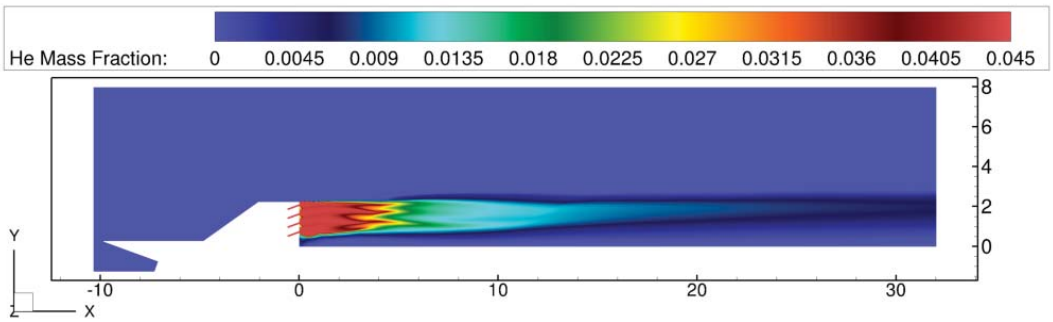

(d) 100% He, ER=0.1

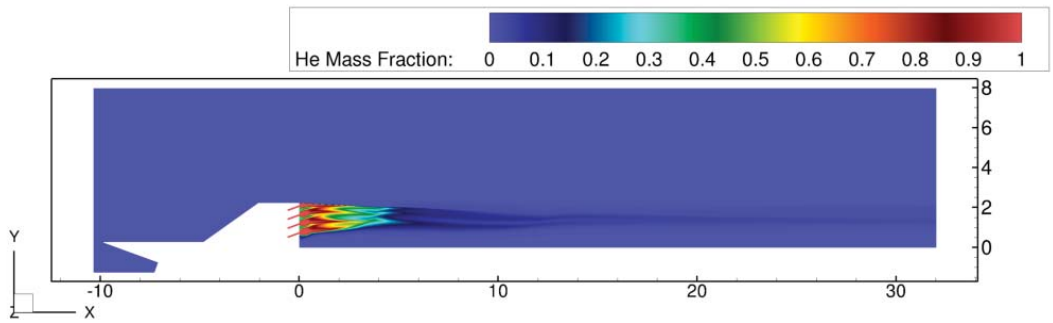

Figure 9: Contours of fuel-simulant mass fraction for several different fuel-simulants and different values of the ER. Plot axis are in inches.

Actually, quite the opposite may be true because of the modifications to the injector and its configuration, and differences in the operating conditions from those previously tested in Baurle et al.[15]. Nevertheless, the current set of simulations with different fuel-simulants and ERs, provided verification that a range of mixing conditions can be observed given a certain length of the flat plate and that the mixing fields are qualitatively similar for pure helium, helium-air mixtures, and hydrogen gases.

As mentioned previously, an ER of 1 and a mixture of 25%-75% helium-air was considered to more closely match the value of the ratio of specific heats, and therefore, the near-injector expansion plumes to those of hydrogen. However, in proportions needed to significantly alter the ratio of the specific heats, the molecular weight of the helium-air mixture is significantly greater than that of either hydrogen or helium. Furthermore, the reduced helium content in this mixture significantly reduces the resolution of the in-stream gas-sampling rake probe measurements used in the experiment. Therefore, while the mixture of helium and air produces a qualitatively comparable mixing flow field to that of pure helium or hydrogen at the same ER, it will likely only be used under special circumstances during the experimental campaign, for example, when the NO-PLIF technique is further verified.

Among the simulations shown in Figs. 8 and 9, the ones with pure helium, ER of 1, and adiabatic and isothermal boundary conditions were used to obtain the surface temperatures and heat fluxes for thermal analysis of the flat plate. The results of these simulations were provided to an external contractor who used the surface loads to design the flat plate and supporting hardware.

The simulations with helium and an ER of 0.1 (also shown in Figs. 8 and 9) and 1.0 were used to define the flow field properties for the analysis of the gas sampling system developed specifically for the EIM project. Moreover, the ER of 0.1 case provided a test case with reduced mass fraction of helium and a nearly fully mixed flow field near the end of the plate. While the gas-sampling system could be readily tested in any mixing flow field by moving the gas-sampling probe vertically across the mixing plume and into the free-stream, the team desired an environment that provided a full range of mixing conditions within the mixing plume.

The CFD data obtained during these simulations were also used to develop and test post-processing and analysis tools. The VULCAN-CFD suite already includes a range of post-processing and performance utilities that can be used with little to no modifications. An example of utilizing these tools for the analysis of the mixing data obtained via the CFD is presented below. The current CFD data is also being post-processed to simulate data expected to be available from the experiments. The simulated experimental data consists of sampling the CFD flow field at the discreet gas-sampling rake probe locations to obtain helium mole fractions, total temperatures, and Pitot pressures. The work is ongoing to develop utilities that can process the simulated data to obtain plume characteristics such as maximum fuel mole fraction, plume area growth, penetration, and others. Work is also ongoing to investigate relationships between plume characteristics obtainable from the experiments and the more quantitative performance metrics such as mixing efficiency, total pressure recovery, and thrust potential discussed below.

The overall performance of an injector configuration can be assessed by computing one dimensional (1D) profiles of quantities such as total pressure recovery, thrust potential, or mixing efficiency. Figure 10 shows these quantities together with the 1D mass-weighted profile of the Mach number. These profiles help to quantify the level of similarity among the mixing fields discussed above. The total pressure recovery is computed by dividing the value of the mass-weighted average total pressure by the free stream value of the total pressure. The thrust potential is computed by the method of Riggins et al.[16] with the isentropic expansion computed to a state where the atmospheric static pressure at an altitude of 125k ft. is used instead of a prescribed virtual nozzle exit area. The mixing efficiency is obtained following Mao et al.[17] The distance on these plots is in inches with the origin representing the injection plane. Consistent with previous observations, the fluctuating values of the Mach number are caused by the refracted shock waves which alter the speed of the mixing flow. These shock waves together with the increasingly mixed flow downstream of the injector cause an unrecoverable drop in the total pressure and thrust potential. The differences in the value of the quantities in Fig. 10 among the cases corresponding to the ER of 1 are all relatively small with Mach number, total pressure recovery, thrust potential, and mixing efficiency varying by no more that 5%,

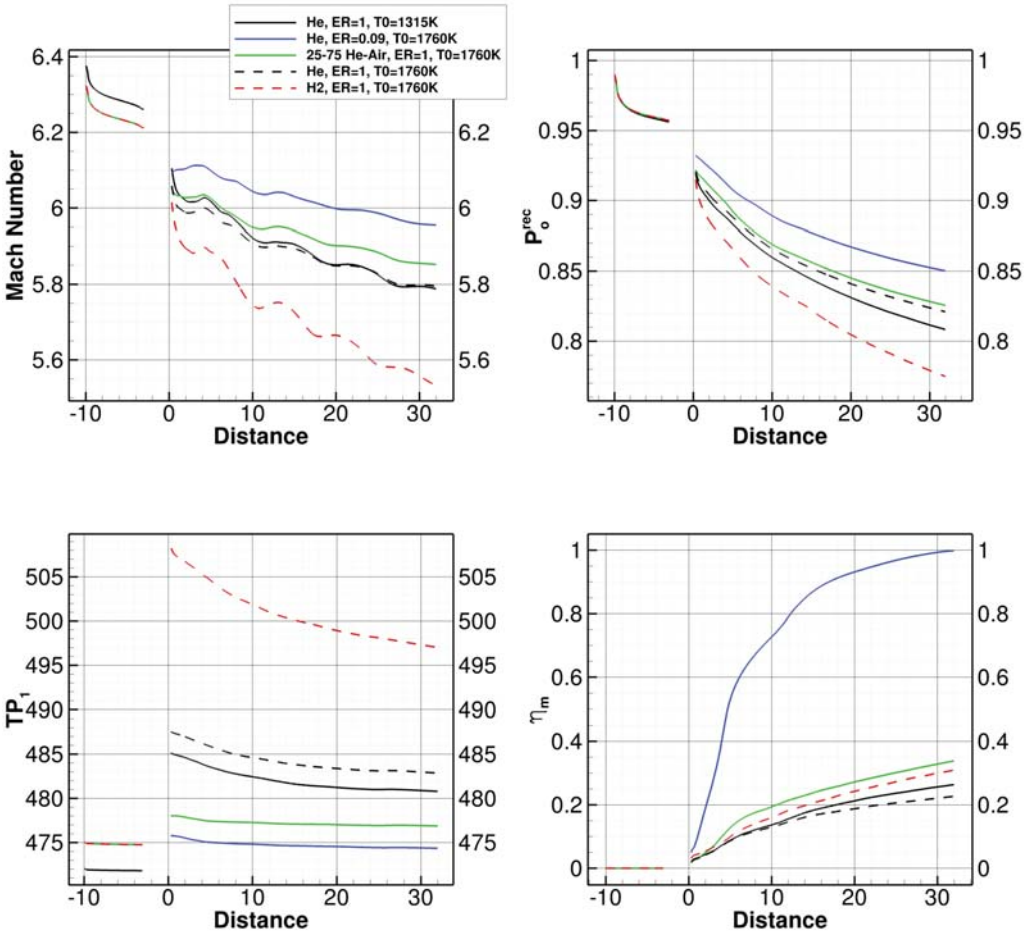

Figure 10: Profiles of the 1D mass-weighted Mach number, total pressure recovery (P_o^{rec}), thrust potential (TP), and mixing efficiency (η_m) vs. distance in inches for several different fuel-simulants, ERs, and total enthalpies.

6%, 6%, and 15%, respectively. These values further support previous assertions that either helium or a helium-air mixtures can be effectively used to simulate hydrogen injection.

In addition to the cases corresponding to the high value of the total enthalpy, the performance of the case with pure helium, ER of 1, and the low value of the total enthalpy is also presented. This additional comparison allows for quantitatively assessing the differences between the flow and mixing fields, total pressure losses, and thrust potentials between the cases corresponding to these different values of the total enthalpy. As can be seen, these differences are also relatively small, with the trend that a reduction in the value of the total enthalpy increases the total pressure recovery but decreases mixing efficiency.

The competing nature between enhancing mixing and minimizing total pressure drop or losses makes the design and optimization process for high-speed injectors challenging and ultimately dependent on the mission requirements. Figure 11 shows the profiles of the mixing efficiency vs. total pressure recovery, rather than the distance, for the same cases shown in Fig. 10. It is clear that the fuel-air mixing is increasing when the total pressure is decreasing. Therefore, to optimize mixing efficiency it is required to understand the physical mechanisms, geometrical features, and configuration layouts which minimize total pressure losses (or thrust potential losses when heat release is considered). Furthermore, because some total

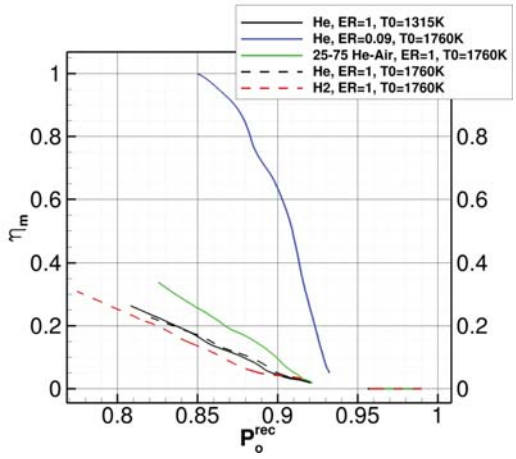

Figure 11: Profiles of the 1D mass-weighted mixing efficiency vs. total pressure recovery (P_o^{rec}) for several different fuel-simulants, ERs, and total enthalpies.

pressure loss is required for mixing to occur, the goal is to find configurations that achieve the minimum amount of total pressure loss for a desired amount of mixing.

EXPERIMENTAL PLATE AND INSTRUMENTATION SHROUD

The next set of simulations was performed to evaluate the interactions between the facility test cabin and the experimental apparatus comprised of the flat plate and the instrumentation shroud. The simulations were specifically used to:

- investigate the interaction between the facility nozzle flow with the flat plate and the instrumentation shroud for the two limiting test cabin back pressure conditions during the experimental run;
- guide the sizing of the width of the flat plate;
- guide the sizing of the length of the jet stretchers;

The following discussion describes the details of the simulations and addresses the above listed items.

To satisfy the above goals a 19 ft. long, 4 ft. internal diameter section of the test cabin directly downstream of the facility nozzle exit plane was gridded and the resulting flow field simulated. The flat plate, measuring 37.2 in. long and 22 in. wide, was mounted 2.5 in. below the facility nozzle center line and 0.4 in. downstream from the facility nozzle exit plane. The back side of the mixing plate has a shroud designed to shield the instrumentation and fuel manifold from the high speed thermal environment. This shroud is 6.5 in. wide and 8 in. high. The shroud has a leading edge with a half angle of 22.4 degrees. The experimental side of the plate is designed so that different injectors can be mounted and tested. For the current calculations, 15 flush-wall injectors each with a diameter equal to that of a single port of the baseline strut injector and located about 6.75 in. downstream from the leading edge of the plate were included. Each injector was fueled with the mass flow rate equal to that of a single port of the baseline strut injector with a nominal ER of 0.1. The injection element was added to investigate the interactions between waves emanating from the facility nozzle exit plane when operating at non-pressure matched conditions, the leading edge of the flat plate, and bow shocks generated by the flush wall injection.

The computational grid contained about 38 million cells and 165 computational blocks. The grid points are highly concentrated around the regions containing the flat plate and the shroud. However, to reduce the total cell count the grid was aggressively coarsened beginning a short distance downstream of the plate.

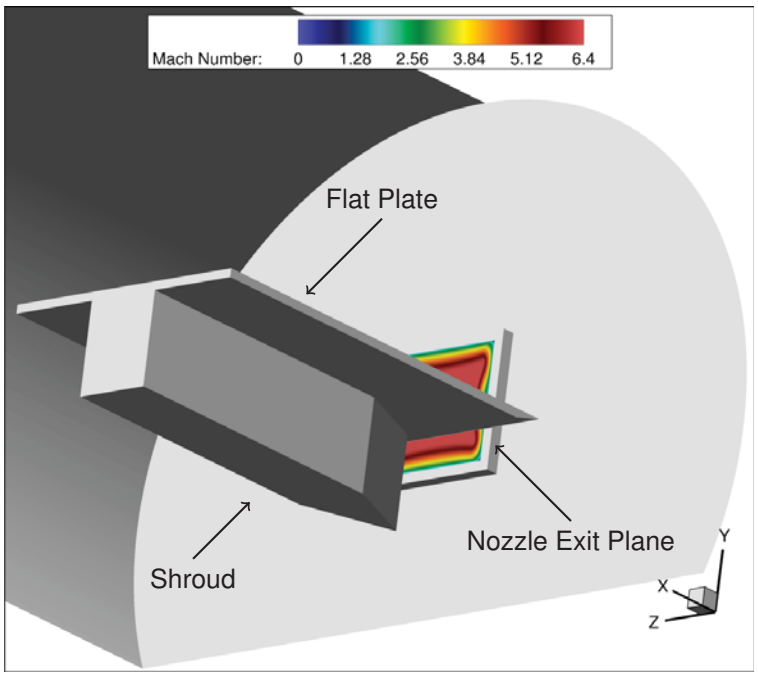

Figure 12: Isometric view of the CFD geometry used to model the plate and the instrumentation shroud inside the test cabin. Also visible is the exit plane of the facility nozzle with the Mach number contours superimposed. Since the y-direction is positive in the plate-normal direction, this image is upside down with respect to schematic in Fig. 1.

To reduce computational time requirements and take advantage of the natural symmetry of this case only half of the geometry was used in the current simulations. However, some graphics were mirrored around the plane of symmetry to improve 3D visualization of the geometry and the simulation results. An isometric view of the CFD geometry showing the flat plate, instrumentation shroud, facility nozzle exit plane colored by the Mach number, and the partial view of the wall of the test cabin are shown in Fig. 12. As before, in the current calculations, the y-direction is positive in the plate-normal direction, therefore the images here are oriented upside down from the actual installation in the facility as shown in Fig. 1. The flow conditions at the facility nozzle exit plane were set to those obtained from the 3D RAS of the facility nozzle. Complete 2D facility nozzle outflow profiles were used. The test cabin walls were set to adiabatic slip walls because the developing boundary layers on the cabin walls were not expected to impact the mixing region on the flat plate or the instrumentation shroud and these boundary conditions reduced the grid resolution and modeling requirements near the cabin walls. The flat plate and its instrumentation shroud were modeled as isothermal non-slip walls with the temperature set to 1000 R. The outflow boundary condition was set to subsonic outflow with a specified back pressure. Two back pressure values of 0.15 psia and 2.0 psia were used. These values represent test cabin pressure conditions expected during the experimental runs at the beginning and end of the run, respectively.

Figure 13 shows the contours of the Mach number in the vertical center plane of the geometry for the two values of the facility back pressure. The images on the left and right correspond to the back pressures of 0.15 psia and 2.0 psia, respectively. Since the pressure at the facility nozzle exit is about 0.25 psia, the case with back pressure of 0.15 psia and 2.0 psia represent under-expanded and over-expanded flow conditions, respectively. Visible in the image corresponding to the 0.15 psia back-pressure case are the oblique shocks initiated by the flat plate's blunt leading edge and the relatively small region of separated flow upstream of the flush wall injectors. The image of the 2.0 psia back pressure case shows a complex interaction between the oblique shocks from the facility nozzle, shock waves generated by the flat plate, and the now much larger separated flow caused by the flush wall injectors. The latter case is clearly not suitable

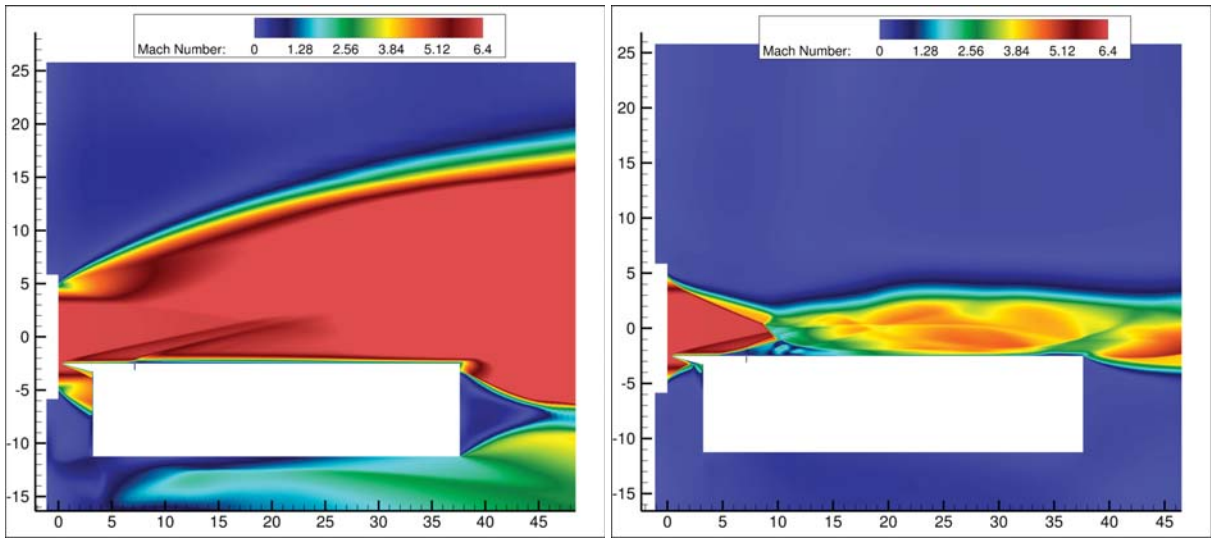

Figure 13: Contours of the Mach number along the vertical center plane of the facility test cabin showing the cross-section of the plate and instrumentation shroud. The two images correspond to the facility back pressure conditions of 0.15 psia (left) and 2.0 psia (right).

for experimental investigations of mixing. Instead, the results of this case were used to confirm the required length for jet stretchers as discussed by Cabell et al.[1]

Figure 14 shows an isometric view with a horizontal semi-transparent contour plane through the center line of the facility nozzle colored by the value of the Mach number. As with the previous figure, the images on the left and right correspond to the two different values of the test cabin pressure of 0.15 psia and 2.0 psia, respectively. This figure shows the span-wise extent of the under- and over-expansion of the flow downstream of the facility nozzle. The two disturbances downstream of the facility nozzle in the figure corresponding to the case of 0.15 psia are the result of oblique shocks originating from the leading edge of the flat plate and separated flow caused by the flush wall injectors.

In addition to elucidating limiting flow environments during the experimental run, the current simulations confirmed that the flat plate width was sufficiently wide to minimize the flow spillage over the side edges, clarified and justified additional requirements for jet-stretchers, provided shroud designers with the bounding aerodynamic and thermal loads impacting the instrumentation shroud, and confirmed the sizing and positioning of the experimental apparatus within the test cabin.

SUMMARY AND CONCLUSIONS

A series of numerical simulations was performed to support the design and development of the EIM project at NASA Langley Research Center. This project aims to investigate the supersonic combustion ramjet (scramjet) fuel injection and mixing physics, improve the understanding of underlying physical processes, and develop enhancement strategies and functional relationships relevant to flight Mach numbers greater than 8. The simulations utilized RAS and included both 2D and 3D calculations of the flow fields within the facility nozzle, calculations of the mixing flow field around an array of strut injectors, and the flow field around the flat plate experimental apparatus and its instrumentation shroud inside the test cabin. A strut injector was chosen as a baseline injector for the calculations and the corresponding preliminary analysis. Pure helium and helium-air mixture were used to determine the efficacy of different inert gases to model hydrogen

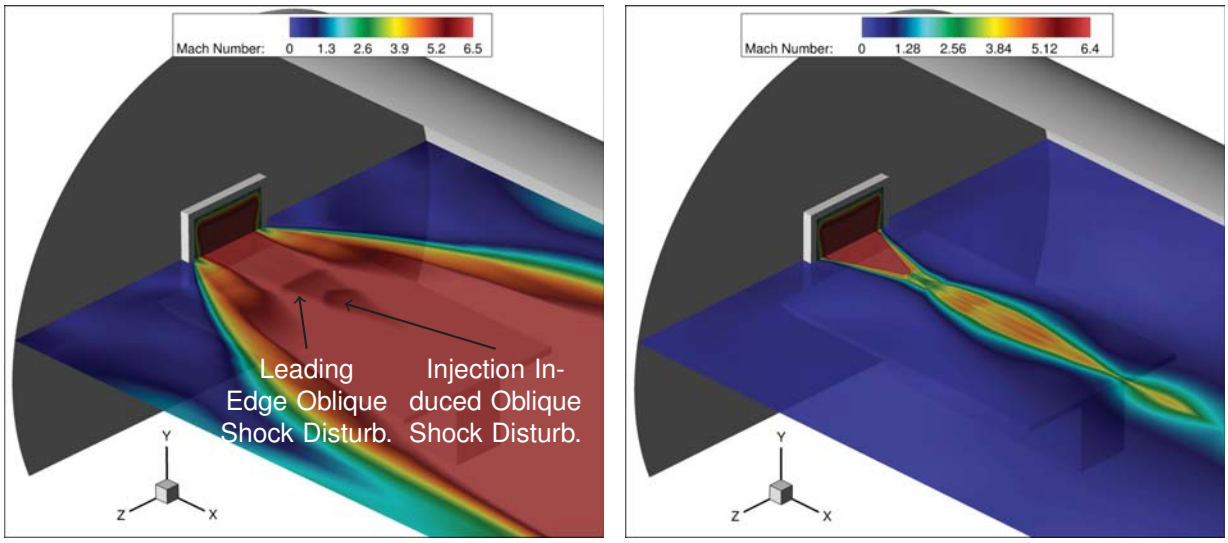

Figure 14: Isometric view of the test cabin with the horizontal plane cutting through the center line of the facility nozzle and colored by the value of the Mach number. The two images correspond to the facility back pressure conditions of 0.15 psia (left) and 2.0 psia (right). Also denoted on the figure are the disturbances caused by the oblique shocks emanating from the flat plate leading edge and the separated area induced by injection.

injection. These results were further analyzed by computing mixing efficiency, total pressure recovery, and stream thrust potential. The simulations provided key data used for the design of the experimental apparatus and instrumentation shroud, assessments of the operational envelope of the in-stream gas sampling rake, and preliminary verification of the non-intrusive temperature measurements based on NO-PLIF. Ongoing work includes the development of common data processing and analysis tools. Practically, every aspect of the experimental design process benefited from the use of the CFD data either directly or via reductions in perceived design risks.

FUTURE WORK

There are several near and long term future goals for the CFD. In the near term, as the experimental data become available, RAS simulations will be rerun at the exact conditions of the experiment and the modeling constants, such at the turbulent Schmidt number, will be calibrated to best match the experimental data, primarily the gas sampled mole fractions of the fuel simulant. These calibrated simulations will then be further processed to gain further insight into the flow structure and flow physics generated by the various injectors and to extract both plume characteristics and mixing metrics. Additionally, once the CFD is reasonably calibrated, the simulations can be further used to explore the relationships between mixing performance and losses that depend on both the flow and geometrical considerations.

In the longer term, the CFD will be coupled with optimization software (currently DAKOTA[18] is considered) to automatically optimize injector configurations based on maximizing the rate of mixing while simultaneously minimizing losses based on either total pressure recovery or the thrust potential metrics. This approach is expected to “drive” configurations to those with minimum pressure loss for a desired amount of mixing. One quantity to optimize, for example, will be the distance between adjacent injectors in an array across a Mach number range.

Most computations will utilize RAS, however, several LES computations will also be used to both validate RAS and investigate the details of the unsteady flow features. Validating RAS via LES is of interest because LES is expected to be more accurate in flows with multi-scale, geometry-induced, strong vortical flows with recirculation zones and flow separation. LES will also be utilized for injection cases explicitly utilizing unsteady effects, such as for cases of pulsed fuel injection.

ACKNOWLEDGMENTS

Authors would like to acknowledge programmatic support provided by the High-Speed Project of the Fundamental Aeronautics Program with Peter Coen as a project manager. Computational resources for this work were provided by NASA Langley Research Center and the NASA Advanced Supercomputing (NAS) Division.

REFERENCES

[1] Cabell, K., Drozda, T. G., Axdahl, E. L., and Danehy, P. M., ***The enhanced injection and mixing project at NASA Langley***, in *JANNAF 46th CS / 34th APS / 34th EPSS / 28th PSHS Joint Subcommittee Meeting*, Albuquerque, NM (Dec. 2014).

[2] Johansen, C. T., Danehy, P. M., Ashcraft, B. F., Bathel, B. F., Inman, J. A., and Jones, B. G., ***Planar laser-induced fluorescence of Mars Science Laboratory reaction control system jets***, J. Spacecraft. Rockets., 50(4):781–792 (2013).

[3] Kidd III, F. G., Narayanaswamy, V., Danehy, P. M., Inman, J. A., Bathel, B. F., Cabell, K. F., Hass, N. E., Capriotti, D. P., Drozda, T. G., and Johansen, C. T., ***Characterization of the NASA Langley Arc Heated Scramjet Test Facility using NO PLIF***, in *30th AIAA Aerodynamic Measurement Technology and Ground Testing Conference*, Atlanta, GA (Jun. 2014).

[4] VULCAN-CFD, ***http://vulcan-cfd.larc.nasa.gov/*** (Nov. 2014).

[5] van Leer, B., ***Towards the ultimate conservative difference scheme. V: A second-order sequel to Godunov's method***, J. Comput. Phys., 32(1):101–136 (Jul. 1979).

[6] Edwards, J. R., ***A low-diffusion flux-splitting scheme for Navier-Stokes calculations***, Comput. Fluids., 26(6):635–659 (Jul. 1997).

[7] Cabell, K. F. and Rock, K. E., ***A finite rate chemical analysis of nitric oxide flow contamination effects on scramjet performance***, Tech. Rep. TP-212159, NASA (2003).

[8] McBride, B. J., Gordon, S., and Reno, M. A., ***Thermodynamic data for fifty reference elements***, NASA Technical Paper 3287/REV1, NASA, Cleveland, OH (Feb. 2001).

[9] Baurle, R., ***Analysis of facility non-equilibrium thermodyamic effects on HIFiRE ground tests***, in *JANNAF 46th CS / 34th APS / 34th EPSS / 28th PSHS Joint Subcommittee Meeting*, Albuquerque, NM (Dec. 2014).

[10] Pulliam, T. H. and Chaussee, D. S., ***A diagonal form of an implicit approximate-factorization algorithm***, J. Comput. Phys., 39(2):347–363 (Feb. 1981).

[11] Menter, F. R., ***Two-equation eddy-viscosity turbulence models for engineering applications***, AIAA J., 32(8):1598–1605 (Aug. 1994).

[12] Wilcox, D. C., ***Turbulence modeling for CFD***, DCW Industries, Inc., La Cañada, CA (2000).

[13] Gaffney, R. and Korte, J., ***Analysis and design of rectangular-cross-section nozzles for scramjet engine testing***, in *42nd AIAA Aerospace Sciences Meeting and Exhibit*, 2004-1137, Reno, NV (Jan. 2004).

[14] Storch, A., Bynum, M., Liu, J., and Gruber, M., ***Combustor operability and performance verification for HIFiRE flight 2***, in *17th AIAA International Space Planes and Hypersonic Systems and Technologies Conference*, San Francisco, CA (Apr. 2011).

[15] Baurle, R. A., Fuller, R. P., White, J. A., Chen, T. H., Gruber, M. R., and Nejad, A. S., ***An investigation of advanced fuel injection schemes for scramjet combustion***, in *36th Aerospace Sciences Meeting and Exhibit*, Reno, NV (Jan. 1998).

[16] Riggins, D. W., McClinton, C. R., and Vitt, P. H., ***Thrust losses in hypersonic engines part 1: Methodology***, J. Propul. Power., 13(2):281–287 (1997).

[17] Mao, M., Riggins, D. W., and McClinton, C. R., ***Numerical simulation of transverse fuel injection***, in *Computational Fluid Dynamics Symposium on Aeropropulsion*, NASA-CP-3078, pages 635–667, NASA, Cleveland, OH (Apr. 1990).

[18] Adams, B., Bohnhoff, W., Dalbey, K., Eddy, J., Eldred, M., Gay, D., Haskell, K., Hough, P., and Swiler, L., ***DAKOTA, a multilevel parallel object-oriented framework for design optimization, parameter estimation, uncertainty quantification, and sensitivity analysis: Version 5.0 user's manual***, Sandia Technical Report SAND2010-2184, Sandia (May 2013).